Influence of Deformation-Induced Martensite on Fatigue Crack Propagation in 304-Type Steels

Z. MEI and J.W. MORRIS, Jr.

This research reports an investigation into the influence of mechanically induced martensitic transformation on the rate of fatigue crack growth in 304-type austenitic stainless steels. Two steels of different composition, 304L and 304LN, were used to test the influence of composition; two test temperatures, 298 and 77 K, were used to study the influence of test temperature; and various load ratios were used to determine the influence of the mean stress. It was found that decreasing the mechanical stability of the austenite by changing composition or lowering temperature reduces the fatigue crack growth rate and increases the threshold stress intensity for crack growth. However, this beneficial effect diminishes as the load ratio increases, even though increasing the load ratio increases the extent of the martensite transformation. Several mechanisms that may influence this behavior are discussed, including the perturbation of the crack tip stress field, crack deflection, work hardening, and the relative brittleness of the transformed material. The perturbation of the stress field seems to be the most important; by modifying previous models, we develop a quantitative analysis of the crack growth rate that provides a reasonable fit to the experimental results.

I. INTRODUCTION

MANY common austenitic stainless steels are mechanically metastable at low temperature and undergo spontaneous transformations when subjected to sufficient stress or strain. The martensitic transformation causes a shape deformation that is evidenced by surface relief effects[1] and a volume change that is dependent on the composition and is ≈2 pct in 304-type stainless steels.[2,3] The strain that occurs ahead of the crack tip during fatigue crack growth in a metastable material induces a partial transformation to martensite, which alters both the microstructure and the stress state at the crack tip, and should, therefore, change the fatigue crack growth rate. It is necessary to understand these changes to design reliable engineering structures and to design or select structural steels with suitable fatigue resistance.

While there have been many research studies on the influence of the mechanically induced martensitic transformation on tensile properties, there is relatively little prior work that addresses its effect on fatigue crack propagation. The bulk of the relevant work[4–12] suggests that the martensitic transformation decreases the crack growth rate. With the exception of Reference 11, however, the fatigue crack growth measurements were confined to the Paris, or power law, region of crack growth. The microstructural mechanisms are not understood. The present research was undertaken to clarify the mechanisms of fatigue crack propagation in metastable austenitic steels. The research included studies of the fatigue crack growth in both the Paris and near-threshold regions in 304-type stainless steels as a function of composition, temperature, and load ratio.

Z. MEI, Research Engineer, and J.W. MORRIS, Jr., Professor, are with the Center for Advanced Materials, Lawrence Berkeley Laboratory, and the Department of Materials Science and Mineral Engineering, University of California at Berkeley, Berkeley, CA 94720.

Manuscript submitted November 28, 1989.

II. EXPERIMENTAL PROCEDURE

A. *Materials*

The materials used in this study were commercial grade AISI 304L and 304LN stainless steels. Their chemical compositions are listed in Table I. They differ primarily in nitrogen content, which is higher in 304LN. Increasing nitrogen raises the yield strength at low temperature (Table II) and stabilizes the austenite phase. Plates of 304L stainless steel were processed in two different ways. The basic material was annealed at 1050 °C for 1 hour, followed by a water quench to create a homogeneous austenite phase. Some of the plates were then rolled 13 pct at liquid nitrogen temperature (LNT) to form a two-phase mixture of austenite and martensite. Plates of 304LN were used in the as-received (annealed and quenched) condition. The average grain sizes of 304L and 304LN were 100 and 70 μm, respectively. Optical micrographs of the annealed 304L and cold-rolled 304L are shown in Figure 1. X-ray diffraction tests confirmed that the annealed 304L and as-received 304LN were essentially pure austenite (γ), while the cold-rolled 304L was about 50 pct austenite and 50 pct martensite (α') with a small admixture of the hexagonal close-packed ε-martensite phase. The tensile properties of the annealed and as-received 304LN were measured and are listed in Table II.[12]

The martensite start temperatures on cooling (M_s) and deformation (M_d) were estimated from the empirical formulas given in References 13 and 14 and are: for 304LN, $M_s < 0$ K, $M_d < 255$ K and, for 304L, $M_s < 38$ K, $M_d < 299$ K. The thermal stability of the annealed 304L steel was confirmed by soaking in liquid helium for more than 2 hours; no α' or ε martensite was detected by X-ray diffraction. The volume fractions of martensite developed during tensile strain at room temperature (RT) and LNT were measured as a function of strain by X-ray diffraction.[12] The results are plotted in Figure 2. Despite the similarity of the computed M_d temperatures, the austenite phase in 304L is very much less stable on mechanical deformation than that in 304LN.

U.S. GOVERNMENT WORK
NOT PROTECTED BY U.S. COPYRIGHT

Table I. Chemical Composition (Weight Percent) of 304L and 304LN Stainless Steels

	Fe	Cr	Ni	Mn	P	S	Si	C	N
304L	bal.	18.7	8.64	1.63	0.021	0.010	0.51	0.024	0.074
304LN	bal.	18.54	9.55	1.77	0.014	0.009	0.78	0.021	0.139

Table II. Tensile Properties of 304L and 304LN Stainless Steels

Materials	Testing Temperature (K)	Yield Strength σ_y (MPa)	Ultimate Tensile Strength σ_u (MPa)	σ_u/σ_y	Elongation (Pct)
304L	298	294	658	2.2	85.5
	77	433	1524	3.5	48.1
304LN	298	341	643	1.89	71.7
	77	724	1476	2.0	51.3

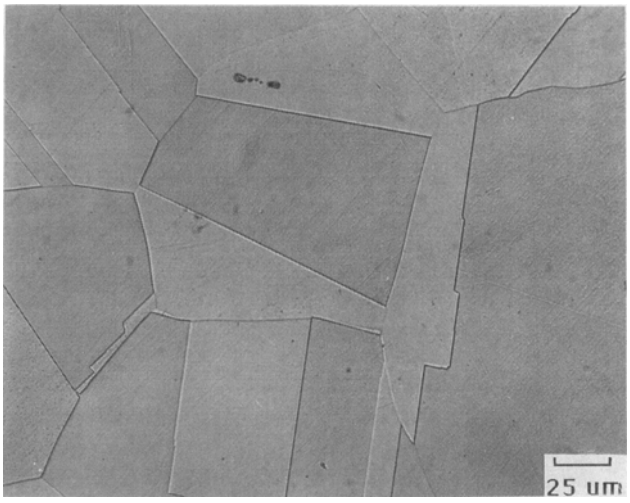

(*a*)

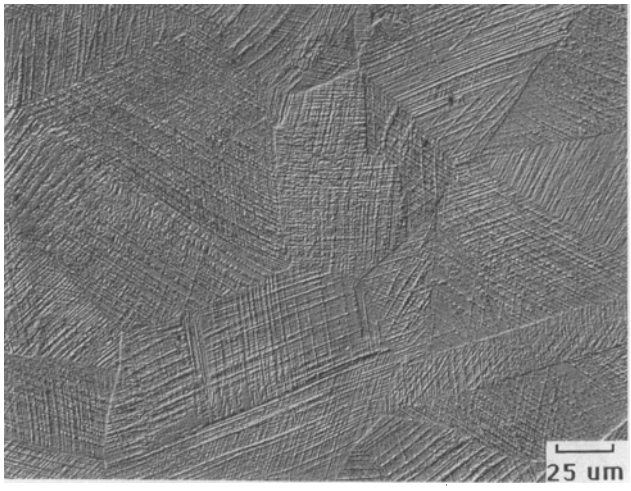

(*b*)

Fig. 1—Microstructures of (*a*) annealed 304L stainless steel and (*b*) annealed 304L after rolling 13 pct at LNT, showing the deformation-induced α' martensite.

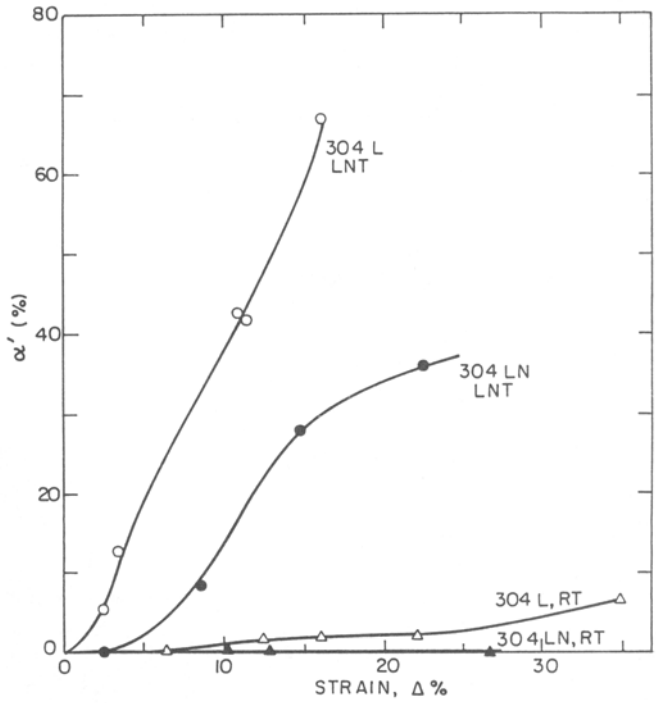

Fig. 2—Relation between the volume fraction of induced martensite, as determined by X-ray diffraction measurement,[12] and the tensile strain for annealed 304L and as-received 304LN stainless steels.

B. *Fatigue Crack Propagation*

Fatigue crack propagation rates were measured according to the procedures recommended in References 15 and 16. The samples were 12.7-mm- and 25.4-mm-thick compact tension specimens of the geometry and size suggested by ASTM standard E647-83.[15] The fatigue crack plane lay in the longitudinal-transverse orientation. The specimens were tested under load control in a hydraulic testing machine with a compression tube frame, using a sine-wave load form and a frequency of 10 to 30 Hz. The cyclic stress intensity (ΔK) was calculated from the crack length and cyclic load as suggested by the ASTM standard.[15] The crack length was monitored continuously using the direct-current electrical potential method.[16,17] The crack length was recorded as a function of cycle number on a strip chart recorder, and the fatigue crack growth rate, da/dN, was determined from the slope of the curve. Fatigue crack growth was monitored over a range of growth rates from 10^{-11} to 10^{-6} m/cycle to sample both the near-threshold and Paris regions. The near-threshold crack growth rates were measured under decreasing ΔK conditions (the "load shedding"

method),[16,18] using a stepwise decrement in ΔK of less than 7 pct per step. At each load level, the crack was allowed to propagate for a distance at least 3 times the computed maximum radius of the plastic zone formed at the previous load level. After establishing the threshold, the load was increased stepwise, and da/dN values were recorded until the specimen sustained general yield. The RT fatigue tests were done in air at about 298 K; the tests at LNT (77 K) were done by immersing the compression tube and specimen in a 25-L Dewar filled with liquid nitrogen.

The extent of crack closure during fatigue crack growth was monitored continuously using the back face strain gage technique.[19,20] In this technique, a strain gage is mounted on the back face of the specimen, and the closure stress intensity, which represents the macroscopic contact of the fracture surfaces during unloading, is determined from the load at which the elastic compliance curve first deviates from linearity.

C. *Optical Microscopy*

The deformation-induced martensite around the fatigue crack was observed after the fatigue test by optical microscopy on samples that were sectioned perpendicular to the crack plane at center thickness. Tests showed that no martensite was induced during grinding or polishing. Two methods were used to reveal the martensite: (1) chemical etching in a solution of 15 ml HNO_3, 45 ml HCl, and 20 ml methanol for about 1 minute, which reveals the grain boundaries and interfaces between martensite and austenite, and (2) painting the surface with ferrofluid,[21,22] which highlights the magnetic α' martensite in the paramagnetic austenite matrix. While all of the optical metallography was done at RT, there was no evidence of martensite reversion during heating from 77 K, and none is believed to occur.[23]

D. *X-Ray Diffraction and Scanning Electron Microscopy*

The fatigue fracture surfaces of the specimens were studied under a scanning electron microscope. The γ-, α'-, and ε-phase fractions in the material near the fracture surface were measured by X-ray diffraction. The relative volume fractions of the three phases were determined by comparing the integrated intensities of the $(200)_\gamma$, $(200)_{\alpha'}$, and $(10.1)_\varepsilon$ peaks.

III. RESULTS

A. *Fatigue Crack Propagation*

To explore the influence of the martensite transformation on the fatigue crack growth rate, the extent of transformation during fatigue was varied in three different ways: (1) by changing the chemical composition from that of 304L to that of 304LN, (2) by lowering the temperature from RT to LNT, and (3) by varying the load ratio. The consequences of these three changes are the following.

1. *Chemical composition*

The measured crack growth rates of 304L and 304LN at 298 and 77 K for the load ratio $R = 0.05$ are plotted in Figures 3(a) and (b), respectively. The fatigue crack growth rates of the two alloys are very nearly the same at RT. However, at 77 K, the crack growth rate of 304L is 10 times slower than that of 304LN at $\Delta K = 10$ MPa$\sqrt{\text{m}}$ and is 4 times slower at $\Delta K = 50$ MPa$\sqrt{\text{m}}$. These results correlate directly with the extent of martensitic transformation in the two alloys. Metallographic studies of the fatigue crack profiles show that at RT, both 304L and 304LN remain essentially austenitic at the crack tip as ΔK is varied from 3 to 40 MPa$\sqrt{\text{m}}$. Hence, the fatigue crack growth rate at RT is not significantly affected by martensitic transformation in either alloy. The fatigue crack growth rates are similar despite differences in the static mechanical properties of the two alloys (Table II). At 77 K, on the other hand, 304L transforms substantially in the strain field at the growing crack tip while 304LN only transforms slightly and only at the higher values of ΔK. As shown in Figure 4(a), very little martensite appears near a fatigue crack in 304LN that grows at ΔK values as high as 15 MPa$\sqrt{\text{m}}$. However, as shown in Figure 4(b), martensite coats a growing crack in 304L even when ΔK approaches ΔK_{th}, and a broad region of extensive transformation is present when ΔK is greater than about 20 MPa$\sqrt{\text{m}}$. The fatigue crack growth rate decreases significantly when the chemical composition is changed to promote deformation-induced martensite.

The fatigue crack growth rates of 304L and 304LN at 77 K at a higher load ratio ($R = 0.5$) are compared in Figure 3(c). The crack growth rate is, again, significantly slower in 304L. The decrease is less at $R = 0.5$ than at $R = 0.05$ (*cf.* Figures 3(c) and (a)). However, the difference in the degree of martensitic transformation is greater. Increasing the load ratio from $R = 0.05$ to $R = 0.5$ for given ΔK results in a larger transformation zone with denser martensite in 304L (Figure 9(a)), while about the same degree of transformation occurs in 304LN.

2. *Temperature*

Figure 3(d) illustrates the effect of decreasing the test temperature on the fatigue crack growth rate in the two metastable steels. The fatigue crack growth rate of 304L at RT, where the austenite phase is stable, is significantly greater than that at LNT, where the alloy undergoes extensive transformation. On the other hand, Figure 3(e) shows that the fatigue crack growth rate in 304LN is relatively insensitive to temperature at lower ΔK values where the transformation is insignificant at both test temperatures. Again, the martensitic transformation reduces the fatigue crack growth rate.

3. *Load ratio*

The influence of the load ratio on the fatigue crack growth rate at 77 K is illustrated in Figures 3(f) and (g). The plot shows that as the load ratio, R, increases from 0.05 to 0.5 (representing a 1.9 times increase in K_{max} for given ΔK), the fatigue crack growth rate curve shifts sharply to the left for the unstable alloy, 304L, but is essentially unchanged for 304LN except at very high ΔK, where some transformation occurs. This result is in agreement with prior work[12] which measured an increase in the fatigue crack growth rate of 304L by a factor of 18 as R increased from 0.1 to 0.75 at 77 K.

An increase in the fatigue crack growth rate with the

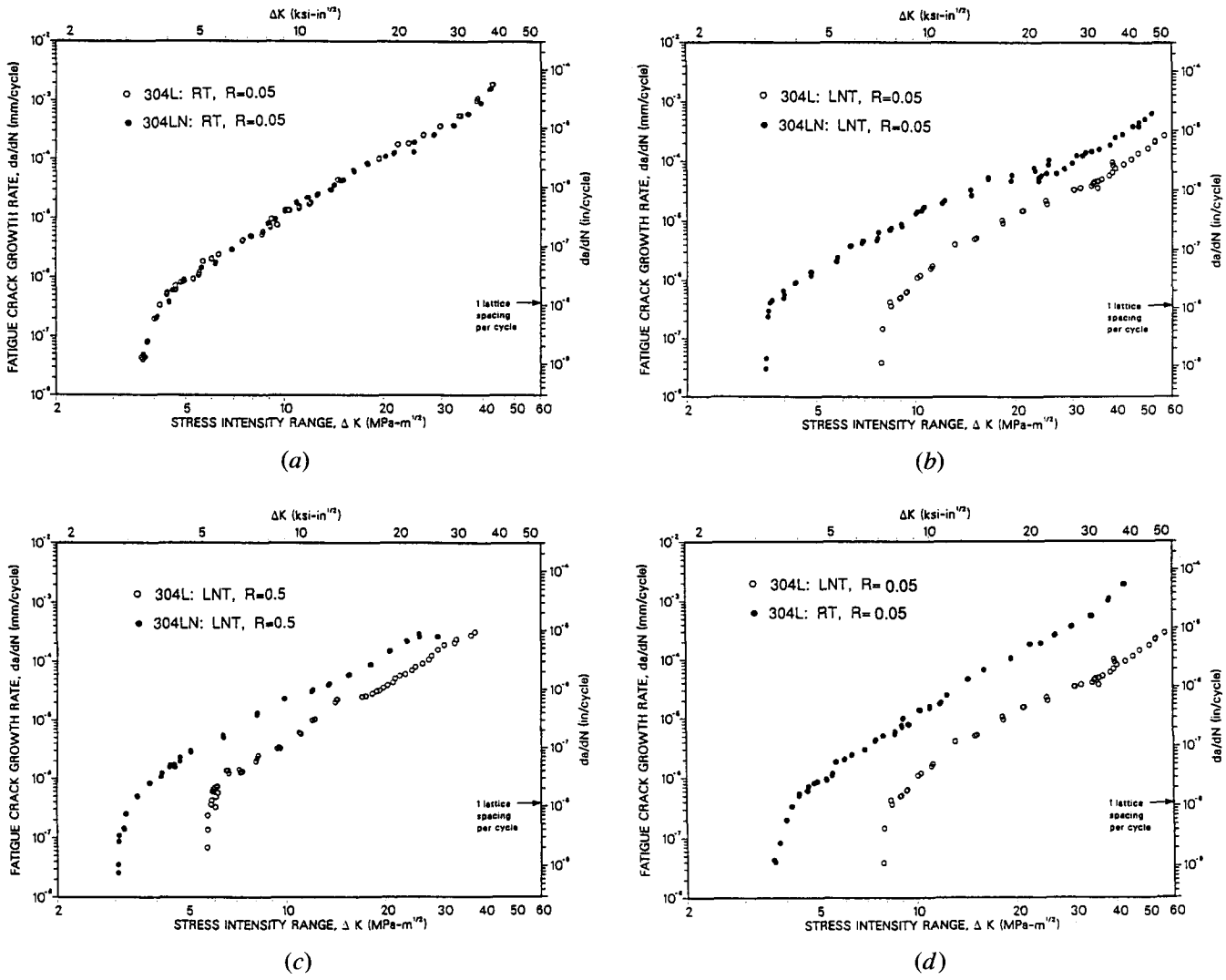

Fig. 3—Crack growth rates as a function of cyclic stress intensity for (*a*) 304L and 304LN austenitic stainless steels tested at RT with load ratio (*R*) 0.05; (*b*) 304L and 304LN steels tested at LNT with load ratio 0.05; (*c*) 304L and 304LN steels tested at LNT with load ratio 0.5; (*d*) 304L steel tested at RT and LNT with load ratio 0.05; (*e*) 304LN steel tested at RT and LNT with load ratio 0.05; (*f*) 304L steel tested at LNT with load ratio varying from 0.05 to 0.5; and (*g*) 304LN steel tested at LNT with load ratio varying from 0.05 to 0.5.

load ratio is a common phenomenon, but the effect is usually small. Figure 5 contains a plot of data drawn from the literature on the fatigue crack growth rates of austenitic steels. The fatigue crack growth rate at given R is normalized by dividing it by the growth rate at $R = 0.1$; the value is approximately the same for all ΔK in the linear, Paris law region of the crack growth curve. In all cases, the fatigue crack growth rate increases with R but by an amount that is significantly greater under conditions where the austenite is relatively unstable. These results suggest that the martensitic transformation exaggerates the load-ratio effect.

The abnormally large R-ratio effect in metastable austenitic steels is surprising since the extent of the martensitic transformation increases with R at given ΔK. The composition and temperature results suggest that the crack growth rate should *decrease* with the extent of the martensite transformation. Taken together, the results suggest that the reduction in the crack growth rate due to the transformation depends on the load ratio; that is, high tensile mean stress lessens and even eliminates the effect of the transformation. Figure 6 includes all of the crack growth rate data taken in research to date. It shows that as the R ratio increases, the crack growth rate of 304L at 77 K approaches that of 304LN and that of 304L at RT where the alloy is stable.

B. *Crack Closure*

Crack closure during the fatigue cycle was measured using the back face strain gage technique described above. The results are plotted in Figure 7. Crack closure was only observed by this technique in the near-threshold region and only when the alloy transformed extensively at the crack tip. Closure occurred in the near-threshold region of both annealed and cold-rolled 304L at LNT but was not observed for annealed or cold-rolled 304L at RT or for 304LN at either temperature. The results are consistent with the suggestion by Suresh and Ritchie[28] that

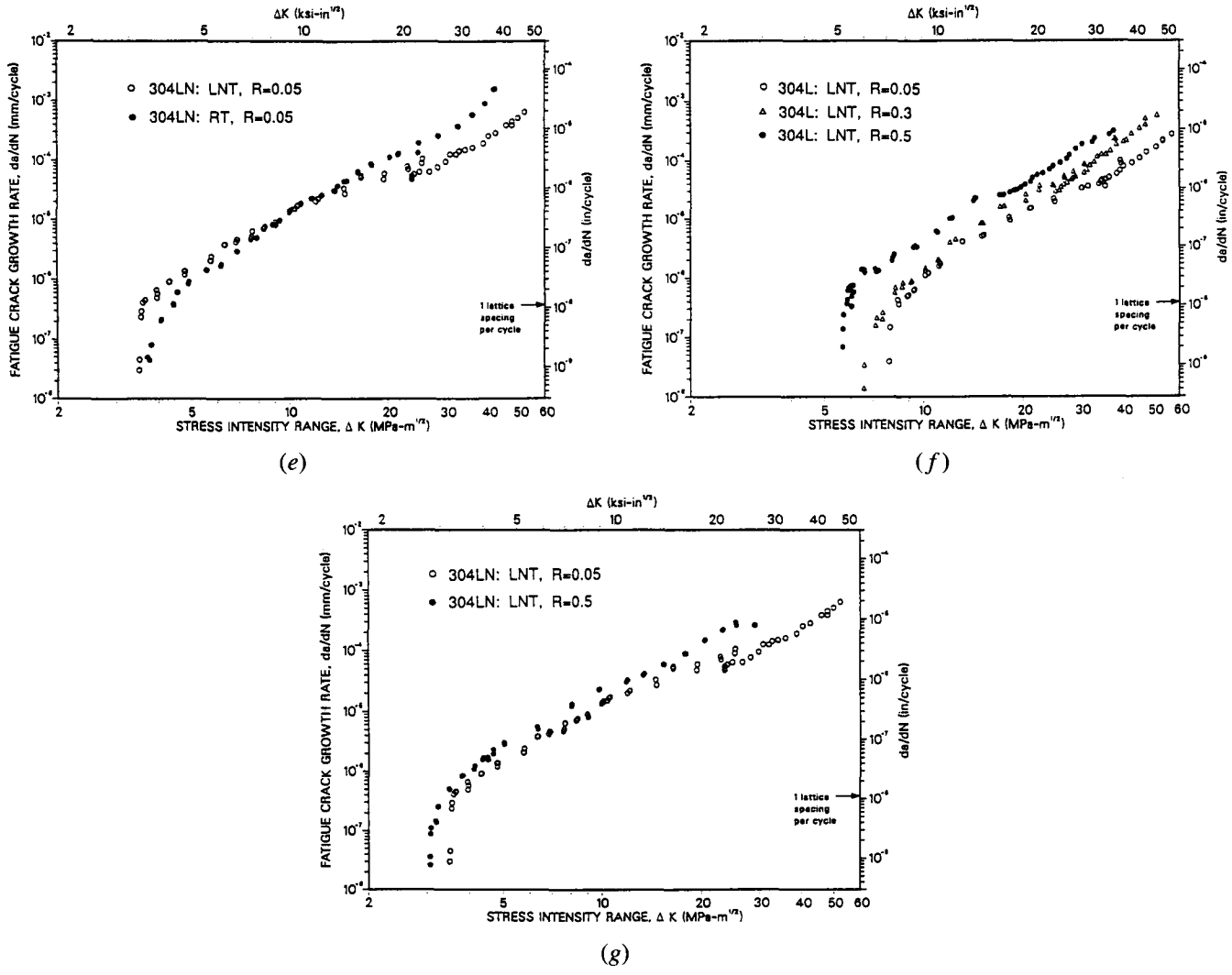

Fig. 3 Cont—Crack growth rates as a function of cyclic stress intensity for (*a*) 304L and 304LN austenitic stainless steels tested at RT with load ratio (*R*) 0.05; (*b*) 304L and 304LN steels tested at LNT with load ratio 0.05; (*c*) 304L and 304LN steels tested at LNT with load ratio 0.5; (*d*) 304L steel tested at RT and LNT with load ratio 0.05; (*e*) 304LN steel tested at RT and LNT with load ratio 0.05; (*f*) 304L steel tested at LNT with load ratio varying from 0.05 to 0.5; and (*g*) 304LN steel tested at LNT with load ratio varying from 0.05 to 0.5.

martensite transformation on the mating surfaces induces crack closure near the threshold. On the other hand, the observed crack closure cannot explain the decreased fatigue crack growth rates at higher ΔK.

C. *Martensite Transformation around the Fatigue Crack*

There are two possible martensitic transformation products in the Fe-Ni-Cr alloy system: the α' body-centered cubic or body-centered tetragonal and ε hexagonal close-packed phases. The $\gamma \rightarrow \alpha'$ transformation involves a 2 pct volume expansion, while the $\gamma \rightarrow \varepsilon$ transformation occurs at nearly constant volume in 304-type alloys. Since both the γ and ε phases are paramagnetic, magnetic etching reveals only the ferromagnetic α' phase. Figure 8 shows the distribution of α' around a fatigue crack. No evidence of ε martensite was found in the X-ray diffraction patterns.

To compare the extent of transformation, the "martensite zone size" was arbitrarily defined to be the distance from the crack surface at which a 10 pct martensite transformation occurred. The measurements were made on etched cross sections and, hence, are somewhat imprecise but do show consistent trends. The data for annealed 304L tested at LNT are plotted in Figures 9(a) and (b) as functions of ΔK and K_{max}, respectively. Since the transformation is driven by the strain, which varies roughly as $K/\sqrt{r}$ near the crack tip, we had expected that the transformation zone size, δ, would be proportional to K_{max}. Figure 9(b) shows that this is not the case. Nor is δ a unique function of ΔK. However, the curves in Figure 9(a) are well fit by an expression of the form

$$\delta = A(\Delta K - C)^2 \qquad [1]$$

where A and C are constants whose values change with R (or, equivalently, with K_{max}). Equation [1] implies that there is a threshold value of the cyclic stress intensity for the transformation.

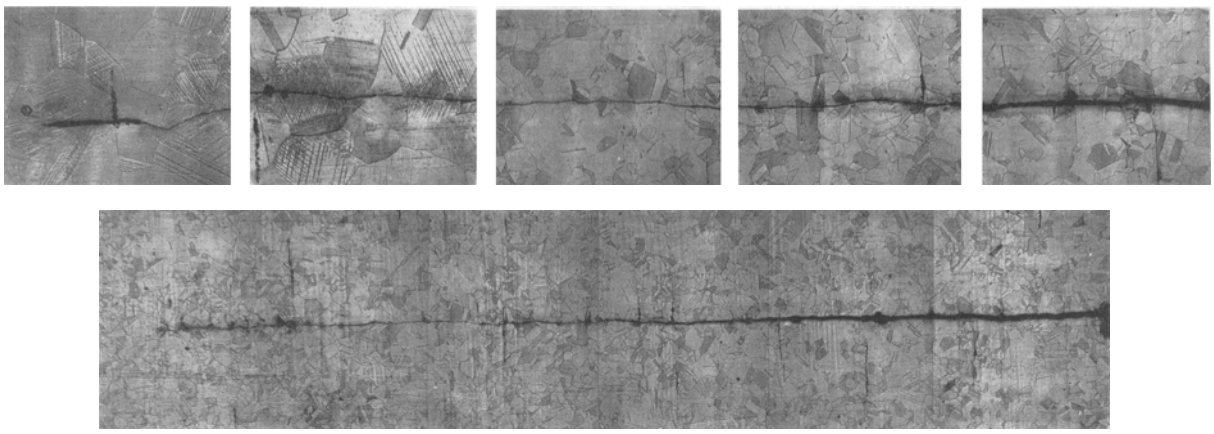

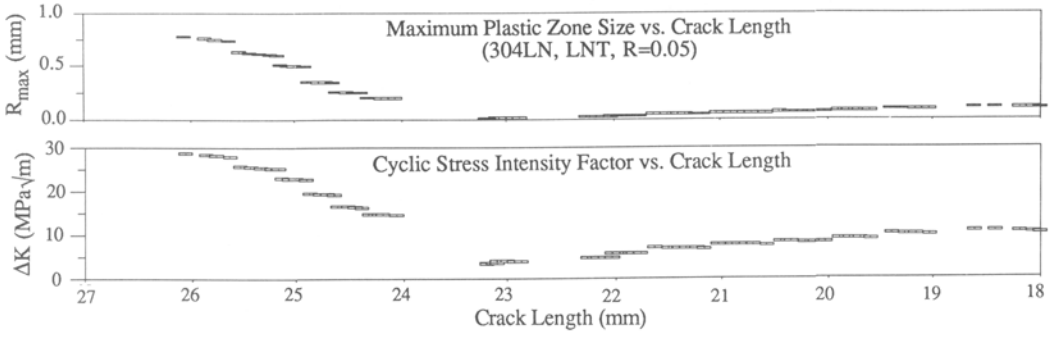

(*a*)

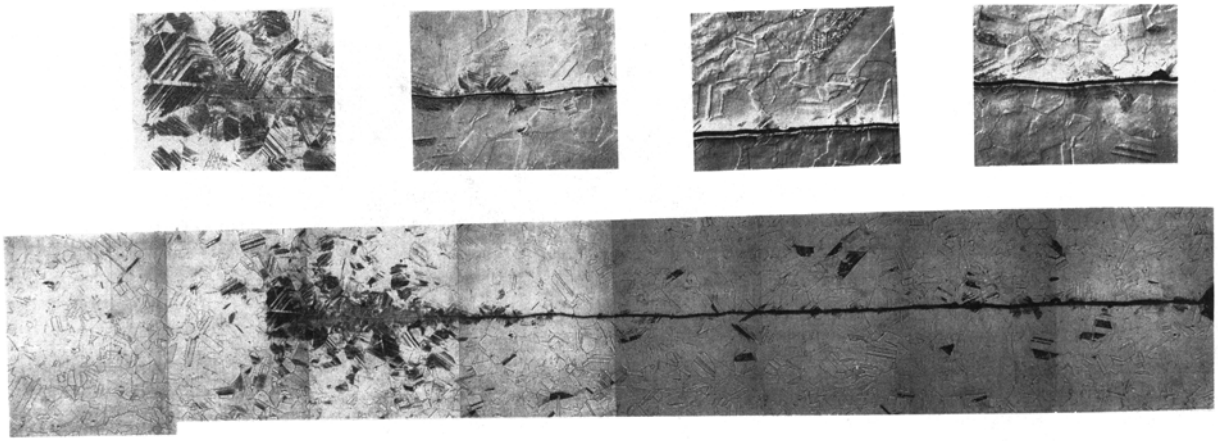

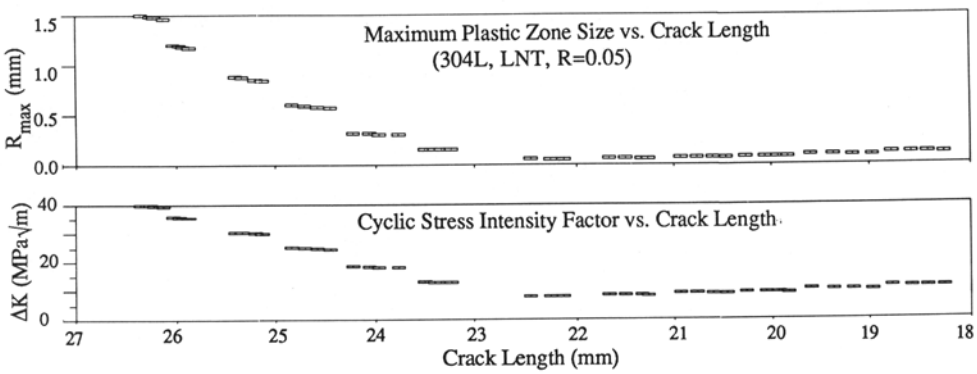

(*b*)

Fig. 4—Optical micrographs of the fatigue crack profiles in (*a*) 304LN stainless steel (*b*) 304L stainless steel tested at LNT, $R = 0.05$, showing deformation-induced martensite. The cyclic stress intensity, ΔK, and the estimated maximum plastic zone size, $[1/(2\pi)]\ (K_{max}/\sigma_y)$, are also indicated. The magnification of each of the upper micrographs is (a) 4 times and (b) 2 times that of the central micrograph, which has a total length of about 9.5 mm.

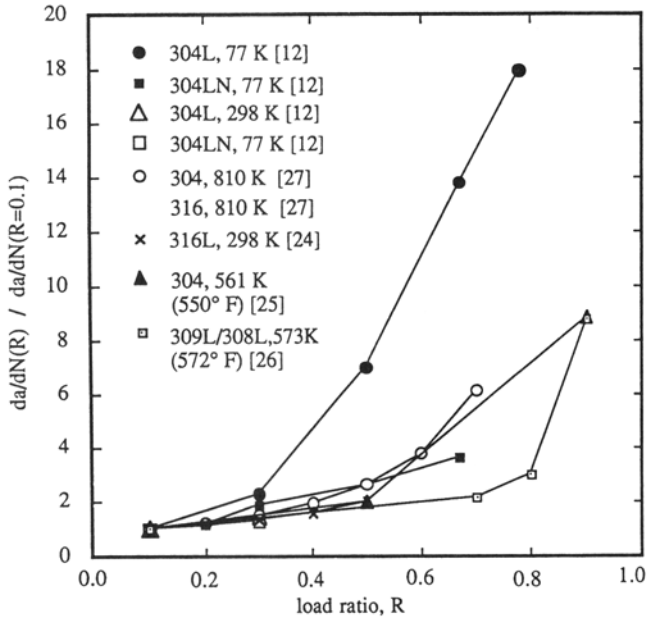

Fig. 5—Normalized crack growth rate (growth rate at R divided by growth rate at $R = 0.1$) as a function of R, showing the abnormally large effect of the load ratio on crack growth rate in 304L at 77 K.

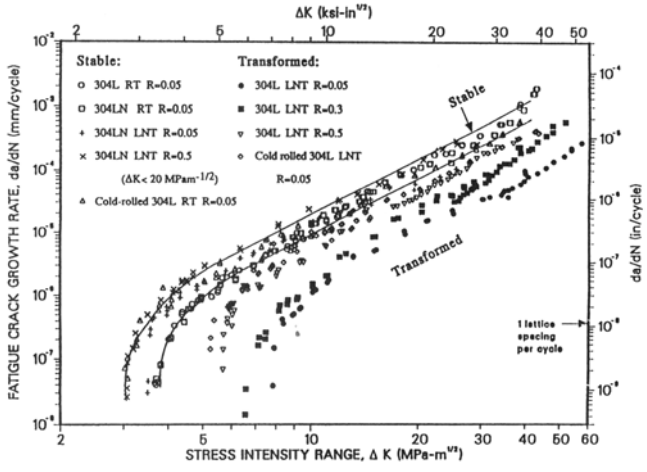

Fig. 6—Summary plot of the fatigue crack growth rate data.

D. *Fractography*

The fatigue crack is transgranular for all conditions studied, as illustrated by the fatigue crack profiles in Figures 4(a) and (b). The fatigue fracture surfaces of 304L (Figure 10(a)) and 304LN (Figure 10(b)) tested at 298 K suggest that significant plastic deformation occurs during fracture. On the other hand, the fatigue surfaces of 304LN (Figure 10(c)) and 304L (Figure 10(d)) tested at LNT contain flat features that resemble quasi-cleavage. The ridges that represent plastic deformation start from the grain boundaries in Figure 10(d), while the anneal twin boundaries in Figure 10(e) do not interrupt the ridges. Recalling the shape of the mechanically induced α' shown in Figures 4(a) and (b), α' features can be identified on the fatigue surfaces in Figures 10(c) and (d). Figure 10(f) shows the form of α' on the fatigue surface of 304L tested at high ΔK and high load ratio where extensive

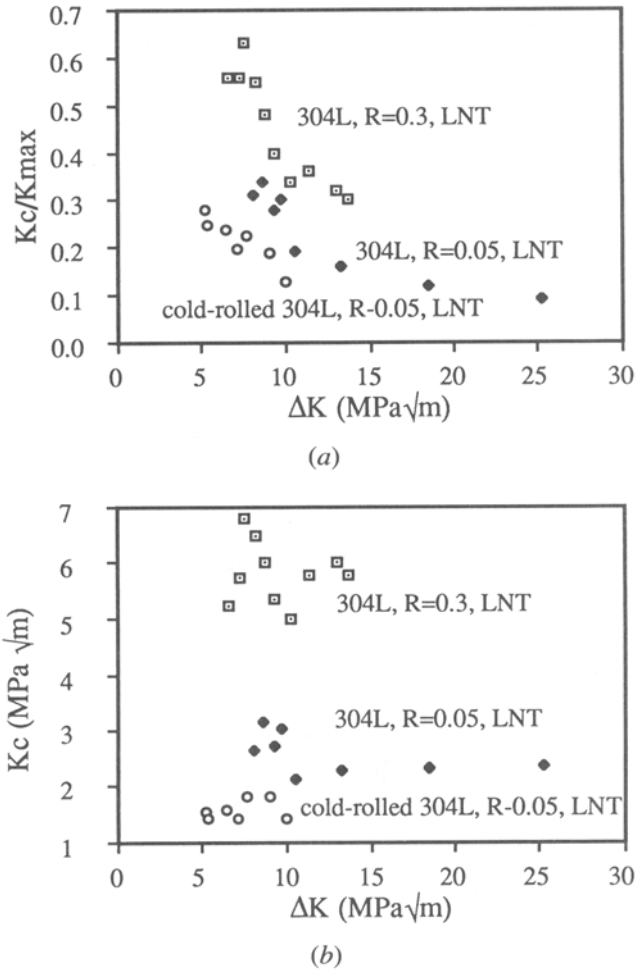

Fig. 7—(*a*) Stress intensity at crack closure, K_c, normalized by the maximum stress intensity, K_{max}, and (*b*) K_c, plotted as functions of the cyclic stress intensity.

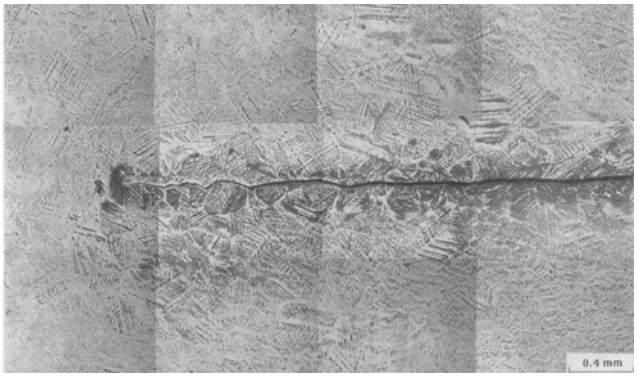

Fig. 8—Optical micrograph of the fatigue crack profile of 304L austenitic stainless steel tested at LNT at $\Delta K = 25$ MPa$\sqrt{m}$. The sample was covered with a thin layer of ferrofluid; 100 Å magnetic particles highlight the magnetic α' martensite.

transformation occurs. It is interesting to notice that the α' on the fracture surface appears as if it were deformed in compression, which suggests the possibility of a microscopic crack closure that is not detected by the back face strain gage technique.

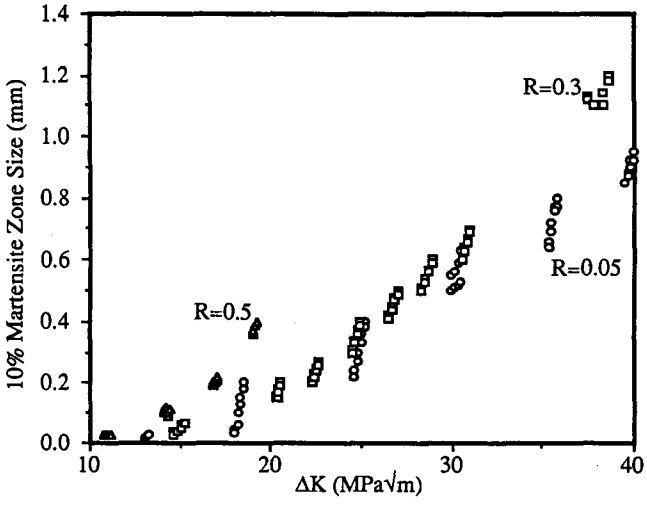

(*a*)

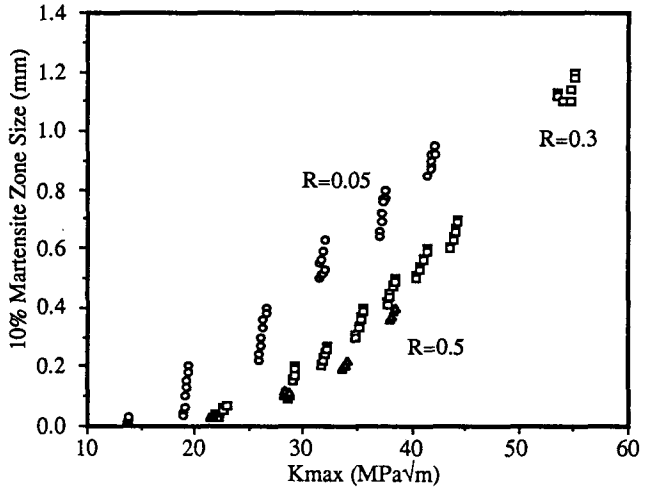

(*b*)

Fig. 9—Metallographically determined martensite zone sizes around fatigue cracks in 304L tested at 77 K at three load ratios (R). The sizes are plotted as functions of (*a*) cyclic intensity (ΔK) and (*b*) maximum stress intensity (K_{max}).

IV. DISCUSSION

Figure 6 includes all of the fatigue crack propagation test data. Two conclusions can be drawn. First, the deformation-induced martensitic transformation increases fatigue resistance. The threshold stress intensity increases, and the fatigue crack growth rate decreases for all ΔK. Second, the beneficial effect of the transformation decreases as the load ratio increases.

A number of mechanisms have been proposed that may contribute to the influence of the martensite transformation on crack growth. These include the incremental strain added by the transformation at the crack tip, the influence of the transformation and the resulting dual-phase microstructure on the crack path, the influence of the transformation on the aggregate mechanical properties of the material at the crack tip, and the influence of the transformation on the fracture mode. We discuss the available models that represent these effects in turn. Among these effects, the transformation strain appears to be the most important.

A. *Influence of the Martensite Transformation on the Crack Tip Stress Field*

The most obvious mechanism that influences crack growth in metastable austenitic steels is the perturbation of the crack tip stress field by the strain associated with the transformation. The $\gamma \rightarrow \alpha'$ transformation in 304-type steels involves both an ~2 pct volume expansion[2,3] and an ~10 pct shear strain.[29] The influence of the volume expansion is the simpler to treat and is analyzed in recent works by McMeeking and Evans[30] and Budiansky *et al.*[31] The influence of the shear component is much more difficult to analyze. The beginnings of a quantitative analysis appear in recent work by Lambropoulos.[32]

1. *Volume expansion*

The constraint of the surrounding elastic material on a dilatant transformed region places that region under compression. If a volume of material that is subjected to a remote cyclic tensile load of amplitude ($P_{max} - P_{min}$) undergoes transformation, both P_{max} and P_{min} are reduced by the associated compressive stress. If P_{min} is large and tensile, the compressive stress does not change the amplitude of the tensile cycle because both P_{max} and P_{min} are reduced by the same amount, but the load ratio changes from (P_{min}/P_{max}) to ($[P_{min} - \Delta]/[P_{max} - \Delta]$), where Δ is the reduction of the tension load by the compressive stress. If P_{min} is a small positive number, it may be reduced to a negative value, in which case the amplitude of the tensile cycle is ($P_{max} - \Delta$) and the load ratio is zero. Since the crack growth rate depends primarily on the amplitude of the tensile cycle and only secondarily on the load ratio, the reduction of the amplitude and load ratio by the compressive stress slows the rate of crack propagation. This effect is qualitatively capable of explaining the influence of the transformation on the crack growth rate: the compressive stress reduces the crack growth rate, but the effect is less pronounced as the load ratio increases, since a higher R ratio means a higher value of P_{min} and a smaller effect on the amplitude of the tensile cycle.

The influence of the volume expansion on the stress field and stress intensity factor is analyzed below in an attempt to quantify its influence on the fatigue crack growth rate. To do this, we must modify previous analyses of the effect.[30,31]

a. *The stress field*

Let a dilatant cylindrical martensite particle be inserted into an infinitely large elastic body. The stress field outside the cylinder can be calculated by modifying the Lamé solution for a thick-walled tube subjected to an internal pressure,[33]

$$\sigma_{rr} = -P\frac{(R_o/r)^2 - 1}{(R_o/R_i)^2 - 1}$$

$$\sigma_{\theta\theta} = P\frac{(R_o/r)^2 + 1}{(R_o/R_i)^2 - 1} \qquad [2]$$

$$\sigma_{r\theta} = 0$$

where R_o is the outside radius and R_i the inside radius. When the ratio R_o/R_i increases without bound,

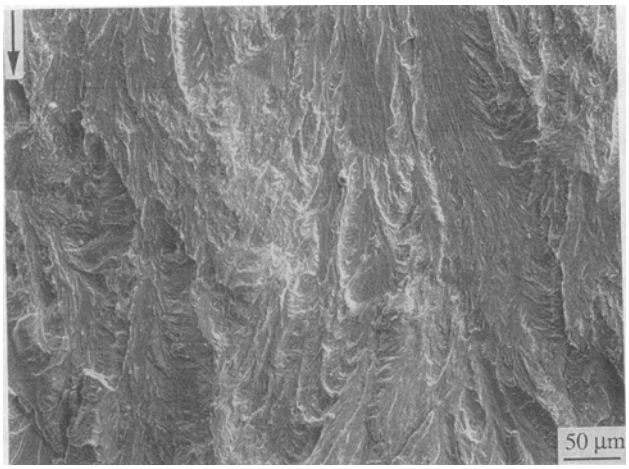

(*a*)

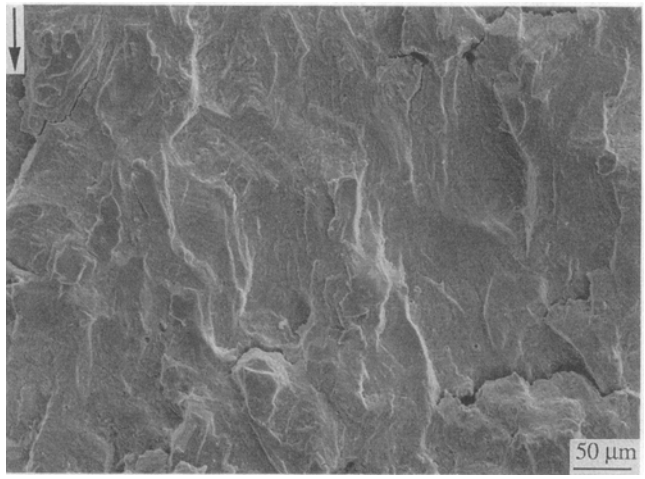

(*b*)

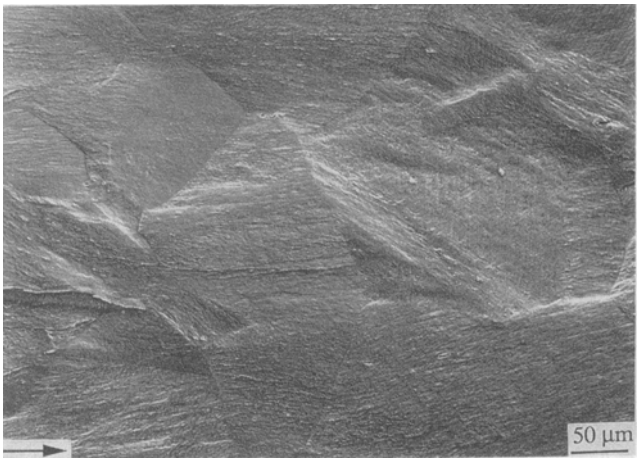

(*c*)

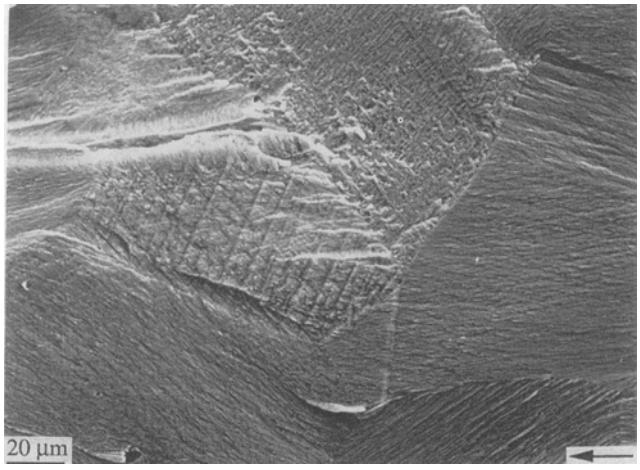

(*d*)

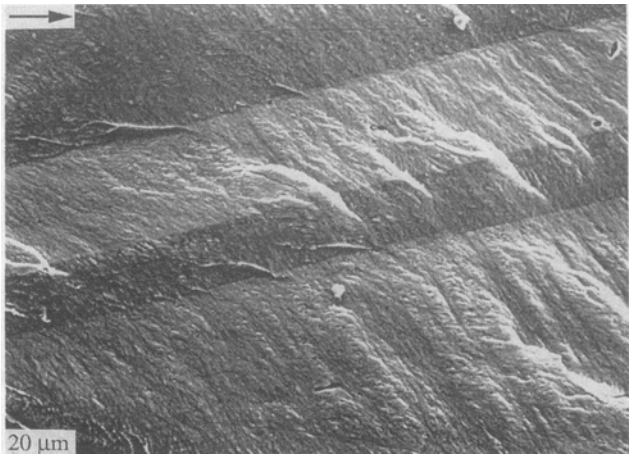

(*e*)

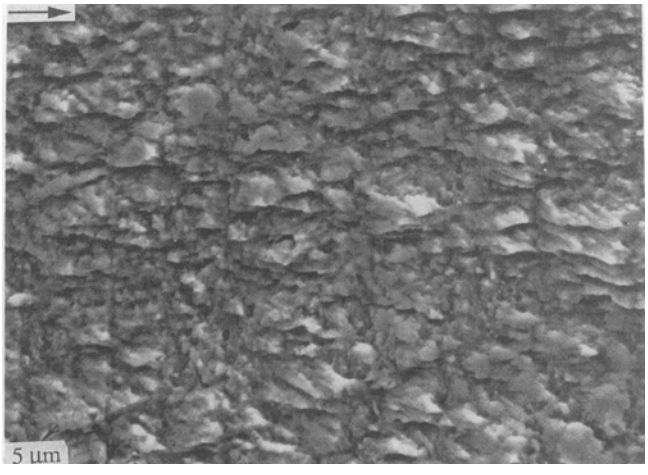

(*f*)

Fig. 10—Scanning electron micrographs of the fatigue fracture surfaces of (*a*) 304LN at 298 K with $R = 0.05$ and $\Delta K = 33$ MPa$\sqrt{\text{m}}$, (*b*) 304L at 298 K with $R = 0.05$ and $\Delta K = 20$ MPa$\sqrt{\text{m}}$, (*c*) 304LN at 77 K with $R = 0.05$ and $\Delta K = 7$ MPa$\sqrt{\text{m}}$, (*d*) 304L at 77 K with $R = 0.5$ and $\Delta K = 8$ MPa$\sqrt{\text{m}}$, (*e*) 304L at 77 K with $R = 0.5$ and $\Delta K = 6.5$ MPa$\sqrt{\text{m}}$, and (*f*) 304L at 77 K with $R = 0.5$ and $\Delta K = 18$ MPa$\sqrt{\text{m}}$.

L'Hospital's rule gives the two-dimensional (2-D) stress field outside the particle as

$$\sigma_{rr} = -P\left[\frac{R_i}{r}\right]^2 \quad \sigma_{\theta\theta} = P\left[\frac{R_i}{r}\right]^2 \qquad [3]$$

The stress field inside the cylinder is constant and hydrostatic

$$\sigma_{rr} = \sigma_{\theta\theta} = -P = -\alpha B\varepsilon^T \qquad [4]$$

where ε^T is the volumetric strain of the martensitic transformation, B is the bulk elastic modulus of the martensitic particle, and α is a parameter, $0 \leq \alpha \leq 1$, whose value depends on the relative stiffness of the particle and the matrix. If the matrix is much stiffer than the martensite particle, $\alpha \approx 1$; while in the other extreme, $\alpha \approx 0$.

If such a cylindrical martensite particle forms directly in front of a growing crack, the driving force for the crack extension is the opening stress, $\sigma_{\theta\theta}$. It follows from Eq. [3] that as the crack approaches the particle, it is subject to a tensile stress that varies as r^{-2} and adds to the cyclic stress at the crack tip due to the macroscopic load. The crack does not experience the compressive field of the martensite transformation until it actually penetrates the particle.

b. *The stress intensity factor*

The stress field at the tip of a crack in a body under an external tensile load is characterized by the mode I stress intensity factor, K_I. The transformation stress, $\sigma_{\theta\theta}$, changes K_I. The amount of the change, K_{tran}, can be found by calculating the stress intensity factor due to $\sigma_{\theta\theta}$ alone and applying the superposition principle. Given the stress field, $\sigma_{\theta\theta}[r, \theta]$, K_{tran} can be found, as proposed in Reference 34, by evaluating an integral of the K_I solution for a pair of concentrated splitting forces on the crack surface. However, the shape of the transformed zone in front of the crack is not simple, and the stress field is difficult to find.

An alternative method for finding K_{tran} was recently proposed by McMeeking and Evans,[30] who used the Eshelby cycle[35] to find the transformation stress and employed a weight function method[34,36] to evaluate the change in stress intensity. In the Eshelby method, the stress and strain fields introduced by a dilatation of magnitude, ε^T, are calculated by summing the fields introduced in a sequence of steps that leads to the final state of the elastic inclusion. A region of the material is cut out and removed from the matrix and then given a volumetric strain, ε^T. This strain is reversed by imposing a surface traction, $\mathbf{T}_c(r, \theta) = -\mathbf{n}(r, \theta)\mathbf{C}\varepsilon^T$, where $\mathbf{C}$ is the elastic matrix of the martensite product and $\mathbf{n}(r, \theta)$ is the outward surface normal. The transformed material is then put back to the matrix and rewelded. Since the material inside the transformed region is under the stress, $-\mathbf{C}e^T$, it relaxes against the unstressed matrix. The relaxation is accomplished by applying a traction, $\mathbf{T}(r, \theta) = -\mathbf{T}_c(r, \theta)$, to the boundary of the particle, since the interface has no traction in its final state. Hence, the stress intensity factor generated by the transformation is equivalent to that generated by a traction, $\mathbf{T}(r, \theta)$, on the boundary of the transformed region. Using the weight function method, the stress intensity factor can be calculated by evaluating the line integral of the scalar product of $\mathbf{T}(r, \theta)$ and the vectorial weight function $\mathbf{h}(r, \theta)$ along the transformed region boundary, S,

$$\Delta K_I = \int_S \mathbf{T}(r, \theta) \cdot \mathbf{h}(r, \theta)\, dl \qquad [5]$$

The weight function, $\mathbf{h}(r, \theta)$, is a measure of the contribution of a unit traction at (r, θ) to the stress intensity factor of an elastic crack.

If the $\gamma \rightarrow \alpha'$ transformation is a pure volume expansion, $\mathbf{T}(r, \theta)$ is equal to $[\mathbf{n}(r, \theta)B\varepsilon^T]$. The solution of $\mathbf{h}(r, \theta)$ for a 2-D infinite solid with a half plane crack was provided in Reference 36:

$$h_x = \frac{1}{2\sqrt{2\pi r}(1-\nu)} \cos\left[\frac{\theta}{2}\left(2\nu - 1 + \sin\frac{\theta}{2}\sin\frac{3\theta}{2}\right)\right] \qquad [6]$$

$$h_y = \frac{1}{2\sqrt{2\pi r}(1-\nu)} \sin\left[\frac{\theta}{2}\left(2 - 2\nu - \cos\frac{\theta}{2}\cos\frac{3\theta}{2}\right)\right] \qquad [7]$$

where ν is Poisson's ratio. The boundary S varies as the crack extends, since fresh material is transformed in the propagating crack tip stress field. McMeeking and Evans[30] assumed that the transformation is driven by the hydrostatic stress and, hence, that the boundary of the transformed zone is a contour of constant pressure:

$$r = \frac{8w}{3\sqrt{3}} \cos^2\left(\frac{\theta}{2}\right) \qquad [8]$$

where w is a measure of the width of the contour, taken to be one-half the zone width. Their result for K_{tran} is plotted along with the computed zone shape in Figure 11; the stress intensity factor is reduced by an amount, $-K_{tran}$, that is zero prior to crack extension, then increases and saturates as the crack enters into the zone. Its asymptotic value is

$$K_{tran} = -0.22\left[\frac{E}{1-\nu}\right] V_f \sqrt{w}\, \varepsilon^T = -0.33\, P\sqrt{w} \qquad [9]$$

where V_f is the fraction of martensite in the zone, E is Young's modulus, ν is Poisson's ratio (approximated as 1/3), and P is the transformation pressure, equal to $BV_f\varepsilon^T$, where B is the bulk modulus.

While Eq. [9] has apparently been used with some success to treat transformation toughening in ceramics, specific calculation shows that the magnitude of K_{tran} is too small to account for the effects observed in the present work. We therefore modified the McMeeking-Evans solution in two respects that are indicated by the detailed state of the material at the growing crack tip.

2. *Zone shape*

The martensite zone shape assumed by McMeeking and Evans is determined by a contour of constant hydrostatic stress. However, the $\gamma \rightarrow \alpha'$ transformation in 304 stainless steels involves a greater shear strain (~10 pct[29]) than volume expansion (~2 pct[2,31]) and, hence, should be more strongly affected by the local shear stress. This is true even when the overall transformation stress is nearly hydrostatic; the formation of a sheared martensite plate

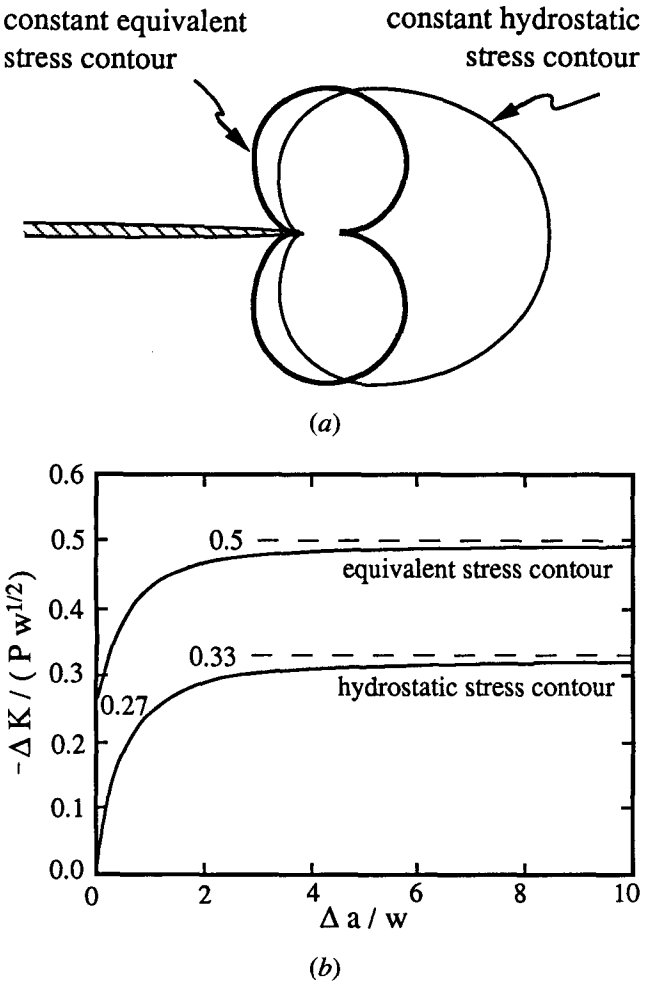

Fig. 11—(*a*) Assumed transformation zone shapes prior to crack propagation: constant hydrostatic stress contour and equivalent stress contour. (*b*) Predicted crack growth resistance (*R*) curves for the two initial zone shapes assuming plane strain and Poisson's ratio, $\nu = 1/3$.

promotes the local formation of others in twinned orientation that tend to cancel the overall shear. Nonetheless, it seems reasonable to assume that the initial transformation, which triggers the process, is determined more by the local shear than by the local hydrostatic stress. This phenomenon is strikingly evident in computer simulations of the stress-induced martensite transformation[37] and is consistent with observations of the martensite zone shape in this and other work[8,38] which show transformation zones that follow shear stress contours much more closely than hydrostatic stress contours.

Using the von Mises measure of shear stress for the plane strain condition,

$$\bar{\tau} = \sqrt{\frac{1}{2}\left[(\sigma_{xx} - \sigma_{yy})^2 + (\sigma_{yy} - \sigma_{zz})^2 + (\sigma_{xx} - \sigma_{zz})^2 + 6\tau_{xy}\right]} \qquad [10]$$

A contour of constant equivalent shear is specified by the relation

$$r = wc(\nu)\cos^2\left(\frac{\theta}{2}\right)\left[3\sin^2\left(\frac{\theta}{2}\right) + (1 - 2\nu)^2\right] \qquad [11]$$

where $c(\nu)$ is a factor that fixes the width, w, of the contour. The shapes of the constant hydrostatic stress and constant equivalent stress contours are sketched in Figure 11(a).

The integral (Eq. [5]) can be solved numerically for K_{tran} as a function of the crack extension for a transformation zone that has the shape given by Eq. [11]. The result is given in Figure 11(b) and shows that a transformation governed by the equivalent shear stress is more effective in reducing the stress intensity factor than a transformation driven by the hydrostatic stress. Moreover, K_{tran} is not zero at the beginning of crack growth. The asymptotic value for the plane strain condition with $\nu = 1/3$ is

$$K_{tran} = -0.5P\sqrt{w} \qquad [12]$$

which is more than a 50 pct greater reduction than in the hydrostatic case.

The reason that the shear-controlled transformation is more effective in reducing the stress intensity becomes apparent when the integral (Eq. [5]) is re-expressed as an integral over the area, A, enclosed by the contour, S,[30]

$$K_{tran} = \int_S B\varepsilon^T n(r,\theta)\cdot\mathbf{h}(r,\theta)\,dl = \int_A B\varepsilon^T\nabla\cdot\mathbf{h}(r,\theta)\,ds$$
$$= \int_A \frac{E\varepsilon^T}{6\sqrt{2\pi}(1-\nu)} r^{-3/2}\cos\left[\frac{3\theta}{2}\right] ds \qquad [13]$$

The integrand in Eq. [13] gives the contribution to K_{tran} from a transformed particle located at (r, θ). Because of the factor, $\cos(3\theta/2)$, in the integrand, transformed particles that are located in a wedge-shaped region in front of the crack (-60 deg $< \theta <$ 60 deg) increase K_{tran}, while particles located outside this region decrease it. When the transformation occurs within a contour of constant shear, a much higher fraction of the transformed region lies in the zone that decreases the stress intensity than when the transformation follows a contour of constant pressure.

Other investigators[32,49,50] have used the weight function technique to compute stress-intensity corrections for transformed zones of still other shapes, such as a shear band profile, maximum principal stress contour, relaxed shear front, and other complicated contours. However, in brittle ceramic materials, the experimentally observed zone shape apparently resembles the hydrostatic stress contour most closely,[51] while in the 304-type stainless steel, the zone shape is given reasonably well by a constant equivalent stress contour.

3. *Martensite distribution*

The calculations leading to Eqs. [9] and [12] assume that the transformation is homogeneous over the region in which it occurs: the transformed fraction is equal to V_f everywhere inside the transformed zone and is zero

outside. In reality, the fraction transformed varies continuously with distance from the crack surface; as shown in Figure 4, for example, the fraction of martensite is high at the crack surface and decreases significantly with distance. It is evident from Eq. [13] that the inhomogeneity of the martensite distribution is important. Because of the factor $r^{-3/2}$ in the integrand, a transformed particle that is close to the crack tip has a much larger effect on the stress intensity than one that is further away.

Equation [12] can be modified to account for the inhomogeneous martensite distribution. Assume that a zone of width w has a martensite volume fraction, V_i, at the crack surface and let it decrease with distance, x, according to the function, $V(x)$, to the value, $V_0 < V_i$, at the zone boundary. To compute the change in stress intensity, we imagine that the zone is created by a sequence of elementary transformations and use the superposition principle. In this picture, the austenite inside the zone of width w transforms to the fraction V_0, then a smaller zone of width x_1 transforms further to $(V(x_1) - V_0)$, a still smaller zone of width x_2 transforms further to create the volume fraction $(V(x_2) - V(x_1))$, and so on, until the whole inhomogeneous transformation is taken into account. The value of K_{tran} in each step can be calculated from Eq. [9] or [12], and the total change is given by the integral

$$K_{tran} = -C\sqrt{w}V_0 + \int_0^w C\sqrt{x}\frac{dV(x)}{dx}dx \qquad [14]$$

where $C = KB\varepsilon^T$ and $K = 0.33$ if Eq. [9] is used and $K = 0.5$ if Eq. [12] is used. If a linear distribution is assumed,

$$V(x) = V_0 + (V_i - V_0)\left[\frac{w - x}{w}\right] \qquad [15]$$

and Eq. [14] becomes

$$K_{tran} = -C\sqrt{w}V_0 - \int_0^w C\sqrt{x}\frac{V_i - V_0}{w}dx$$

$$= -C\sqrt{w}V_0 - \frac{2}{3}C\sqrt{w}(V_i - V_0) \qquad [16]$$

The value of V_0 is the martensite fraction at the transformation zone boundary (10 pct by definition in the present case), while the value of V_i is the martensite fraction at the crack surface, about 50 pct by X-ray diffraction measurement. The distribution of martensite can have a significant effect. For the conditions stated, K_{tran} is about 25 pct larger than it would be if the martensite fraction were homogeneous and equal to its average value.

Given the assumption of a shear-controlled transformation and a linear transformation profile, K_{tran} can be calculated if the transformation zone width, w, is known. In the present work, we found the zone width experimentally for 304L at 77 K for three values of the load ratio. The results are plotted as a function of ΔK in Figure 9. After the fatigue tests, transformation zone sizes were measured by optical microscope as a function of ΔK (Figure 9). It was found that the three sets of data in Figure 9(a) could be fit by a relation of the form

$$w = A(\Delta K - C)^2 \qquad [17]$$

where the values of A and C depend on the load ratio, R. Substituting this result into Eq. [16] yields K_{tran} as a function of ΔK. The resulting values of K_{tran} are plotted in Figure 12, along with the values of K_{max} and K_{min}.

As shown in Figure 12, the magnitude of K_{tran} increases with ΔK, essentially because a higher ΔK causes a more extensive transformation. On the other hand, the stress intensity at crack closure, K_c, that is measured by the back face strain gage is nearly independent of ΔK.

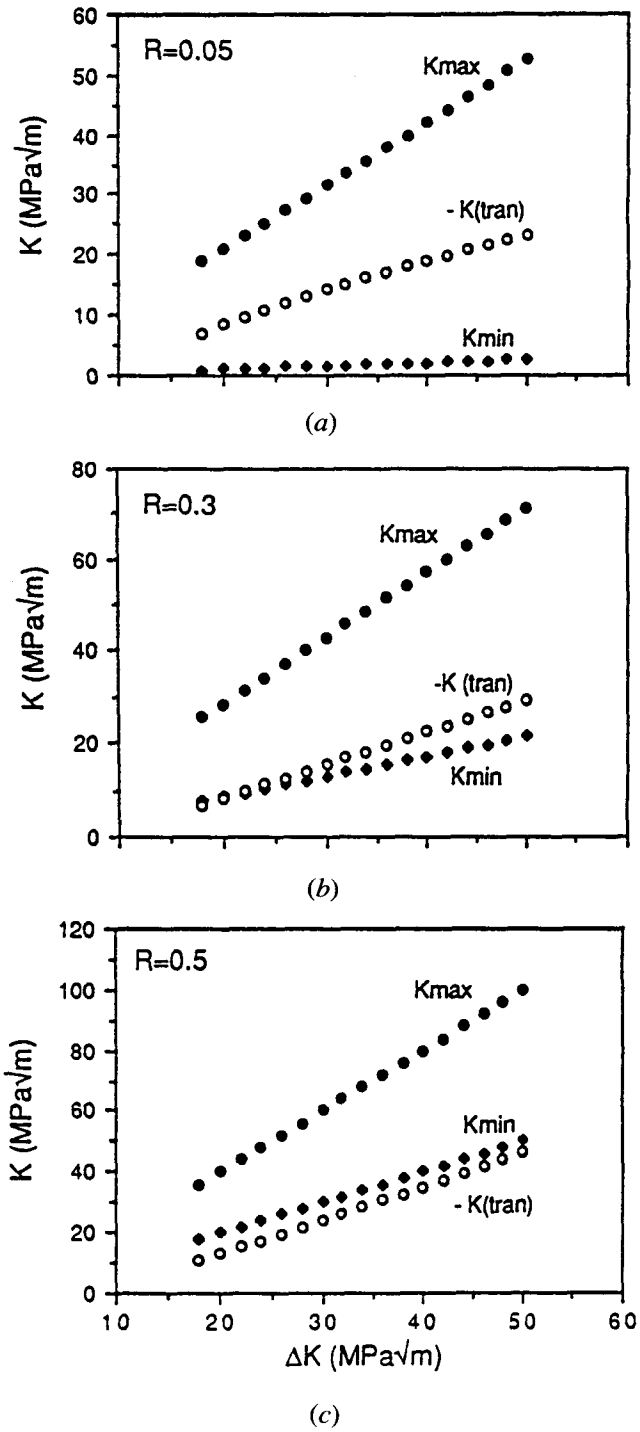

Fig. 12—The reduction of stress intensity factor, $-K_{tran}$, is calculated from Eq. [12] and the transformation zone size plotted in Fig. 9(a) and plotted against the cyclic stress intensity (ΔK) for 304L tested at 77 K for load ratios (R) of (*a*) 0.05, (*b*) 0.3, and (*c*) 0.5. The maximum and minimum stress intensity factors are also plotted for comparison.

These results are superficially inconsistent, since the crack should close at its tip when $K = |K_{tran}|$, but closure is not observed until the stress intensity reaches the value $K = K_c$, which is greater than $|K_{tran}|$ when ΔK is near the threshold but is much smaller at larger values of ΔK. It does not seem reasonable that the discrepancy is simply due to the approximations in the calculation of $|K_{tran}|$; however the transformation effect is calculated, the increased martensite fraction should lead to a higher value of $|K_{tran}|$ and, hence, to earlier crack tip stress relaxation at higher ΔK. We suspect that the discrepancy (and the relatively constant value of K_c) is due to the fact that the back face strain gage measures a qualitatively different phenomenon: the macroscopic closure of the crack over a length sufficient to produce a measurable increase in the modulus. The effect of K_{tran}, on the other hand, is local and specific to the crack tip itself; when $K = |K_{tran}|$, only the very tip of the crack is relaxed. The macroscopic closure, K_c, reflects a number of phenomena, such as the crack roughness; the transformation may not determine its value. On the other hand, the relaxation at the crack tip itself is determined by K_{tran} and can induce closure at the crack tip, essentially removing the driving force for crack growth, even when the crack remains open in a more macroscopic sense.

From this perspective, the effective cyclic stress intensity, ΔK_{eff}, is limited by the larger of three terms: the minimum stress intensity, K_{min}, the stress intensity for macroscopic closure, K_c, and the transformation stress intensity, $|K_{tran}|$. If K_{min} is the largest of the three, the crack never closes. If K_c is the largest, the lips of the crack touch, possibly at a position slightly away from the crack tip, and relax the crack tip stress concentration. If $|K_{tran}|$ is the largest, the stress intensity is relaxed locally at the crack tip. The cyclic stress intensity that should be used in the crack growth law is, then,

$$\Delta K_{eff} = K_{max} - \max\{K_{min}, K_c, |K_{tran}|\} \qquad [18]$$

To test this hypothesis, the fatigue crack growth curves given in Figures 3(f) are replotted to show the fatigue crack growth rate as a function of the effective stress intensity (ΔK_{eff}) in Figure 13. While the curves do not completely coalesce, they agree much more closely with one another. Since ΔK_{eff} is determined by K_{tran}, whose value is known only approximately, over most of the range plotted, the agreement seems reasonably good.

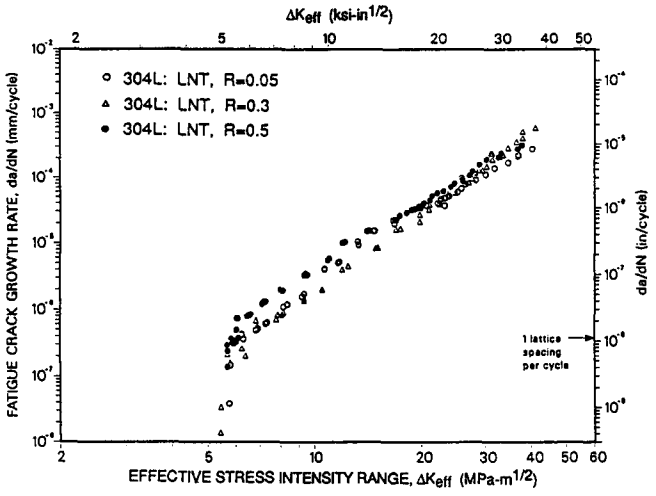

Fig. 13—Crack growth rate as a function of the effective cyclic stress intensity for 304L tested at 77 K at three levels of the load ratio.

We note finally that the above calculation is based on the linear elastic theory and becomes inaccurate when there is substantial deformation at the crack tip. An estimate of transformation toughening based on J-integral methods has been reported recently[52] and may eventually provide a more accurate analysis for ductile metals. However, it is not straightforward to modify this approach to treat fatigue crack propagation. So long as the transformation zone size is much smaller than the crack length and specimen geometry sizes, as it ordinarily is in fatigue and is in the specific case studied here, the stress intensity factor calculation should be valid.

4. *Shear strain*

The calculation that is made above considers only the volume expansion term in the martensite transformation strain. The shear strain in the transformation should also reduce the stress intensity at the crack tip. Unfortunately, this effect is very difficult to estimate quantitatively. The formation of a martensite particle in a particular variant tends to trigger the formation of adjacent particles in variants with compensating shears. Only the net shear affects the overall strain field. The beginnings of an analysis of this effect were made by Lambropoulos,[32] who assumed that the locations and fractions of the different variants of martensite adjust to eliminate the deviatoric component of the macroscopic stress. He was then able to estimate a net value for the transformation strain from this assumption, with the additional approximation that the martensite particles are ellipsoid, so that Eshelby's solution for the elastic field[35] could be employed. The validity of the assumptions made in this analysis is not at all clear, and the results of the calculation for K_{tran} are very sensitive to the assumed orientation of the martensite particles. However, he concludes that the effect of the shear can be large; K_{tran}, due to the shear strain, can be double that due to volume expansion alone.

Since the particle orientation in our fatigue experiments was not regular, it is not clear how to apply his results to our case, and we did not attempt to do so. Nonetheless, we are continuing to investigate the influence of the shear strain.

B. *Other Mechanisms*

Metallurgical effects, besides the perturbation of the crack tip stress, may also influence fatigue crack growth in a material that undergoes transformation. The following were specifically investigated.

1. *Dual-phase microstructure*

The transformation at the crack tip creates a $\gamma + \alpha'$ dual-phase structure and therefore changes the inherent crack growth resistance of the material ahead of the crack tip. To test this effect, a $\gamma + \alpha'$ structure (Figure 1(b)) was produced artificially by cold rolling and tested in fatigue. The results are compared to those for annealed 304L and 304LN in Figure 14. The extent of additional transformation was monitored; it is negligible at RT and small at 77 K. The results of crack closure measurements for the dual-phase specimen are shown in Figure 7.

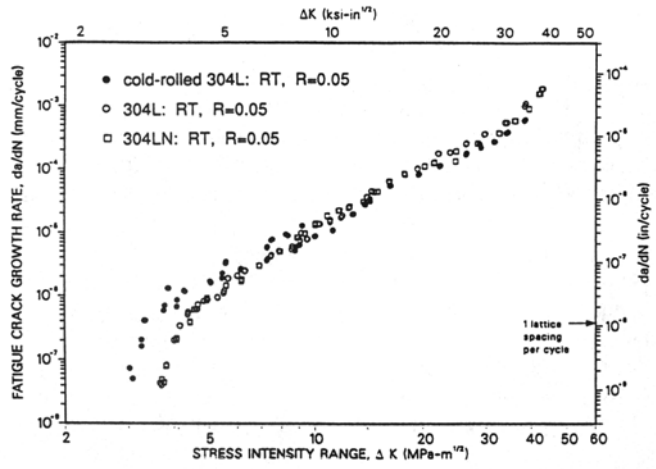

(a)

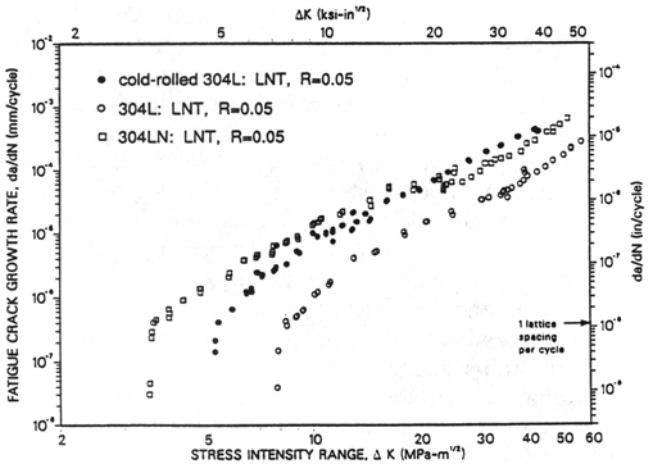

(b)

Fig. 14—Crack growth rate as a function of cyclic stress intensity for cold-rolled 304L, annealed 304L, and as-received 304LN austenitic stainless steels tested with load ratio (R) 0.05 at (a) RT and (b) LNT.

The dual-phase specimen exhibits a fatigue crack growth rate in the Paris region that is close to that in stable austenite, in agreement with previous results that suggest that crack growth rates in the Paris region are relatively insensitive to the microstructure.[39,40] The threshold behavior is affected, as is expected from the change in the stress intensity for crack closure. The fatigue crack growth rate in the dual-phase microstructure is greater than that in metastable (γ) 304L at 77 K, which provides further evidence that the decreased crack growth rate in 304L at 77 K is specifically due to the concurrent martensite transformation.

2. *Crack deflection*

As shown in Figure 15, the crack tends to extend between the martensite laths when material in front of it has transformed extensively. This tendency produces a wavy, zigzag crack path. It has been established in the literature that a crack under a K_I loading advances with a slower speed along a zigzag path than along a flat path. This is because (a) the crack moves through a longer distance along a zigzag path than along a flat path for the same projected length and (b) the externally applied tensile opening loading (K_I) changes to the tensile opening plus sliding loading ($k_1 + k_2$) near the crack tip if the crack deviates from the direction normal to the loading axis. The two effects can be evaluated quantitatively on the basis of the model given in Reference 41.

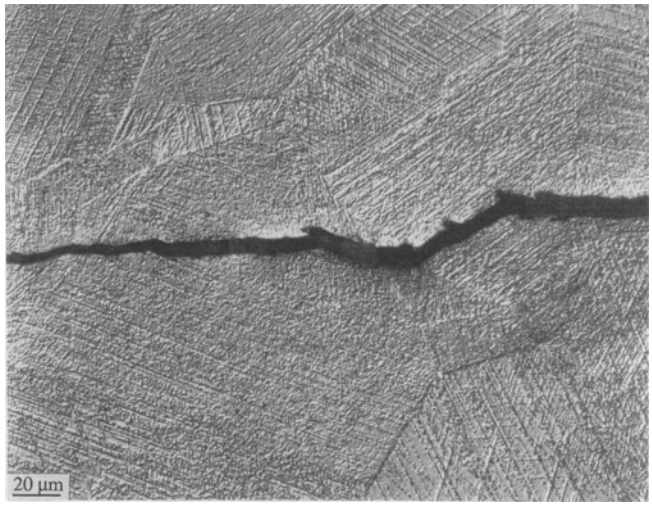

Fig. 15—Optical micrograph of a crack that propagated in an extensively transformed area, showing that a tendency for crack extension between martensite laths produces a zigzag crack path.

Let da/dN and $(da/dN)_1$ represent the respective crack growth rates with and without deflection, and let ϕ denote the angle of deflection from the normal direction to the loading axis. The reduction of crack growth rate due to effect (a) is given in Reference 41 as

$$\frac{da}{dn} = \cos\phi\left[\frac{da}{dn}\right]_1 \qquad [19]$$

The local stress intensities, k_1 and k_2, of a deflected crack can be expressed as functions of the mode I and II stress intensities due to the external load, K_I and K_{II},[42,43]

$$\begin{aligned} k_1 &= a_{11}(\phi)K_I + a_{12}(\phi)K_{II} \\ k_2 &= a_{21}(\phi)K_I + a_{22}(\phi)K_{II} \end{aligned} \qquad [20]$$

The first-order solutions for the $a_{ij}(\phi)$[44] are very close to the exact solutions[43] and are

$$\begin{aligned} a_{11}(\phi) &= \cos^3(\phi/2) \\ a_{21}(\phi) &= \sin(\phi/2)\cos^2(\phi/2) \\ a_{12}(\phi) &= -3\sin(\phi/2)\cos^2(\phi/2) \\ a_{22}(\phi) &= \cos(\phi/2)[1 - 3\sin^2(\phi/2)] \end{aligned} \qquad [21]$$

When K_{II} is zero, as it is in the case of interest to us, Eqs. [20] become

$$k_1 = \cos^3(\phi/2)K_I, \qquad k_2 = \sin(\phi/2)\cos^2(\phi/2)K_I \qquad [22]$$

According to the coplanar strain energy release rate

theory,[45] the effective driving force for the crack propagation is

$$k_{\text{eff}} \approx (k_1^2 + k_2^2)^{1/2}$$
$$= [\cos^6(\phi/2) + \sin^2(\phi/2)\cos^4(\phi/2)]^{1/2} K_I \quad [23]$$

The maximum value of ϕ measured in these tests was about 30 deg; the minimum k_{eff} calculated from Eq. [23] is $0.933K_I$. It is easy to see that in the case of cyclic loading, $\Delta k_{\text{eff}} = 0.933\Delta K_I$. Substituting Δk_{eff} into the Paris law equation, we have

$$\frac{da}{dn} = A(\Delta k_{\text{eff}})^n = A(0.933)^n(\Delta K)^n \quad [24]$$

For 304L steel, n is roughly equal to 3.7. Therefore, the growth rate of a deflected crack is 0.77 ($\approx 0.933^{3.7}$) times that of a linear crack. If Eq. [19] is also taken into consideration, the crack grows in its irregular path at a rate about 0.67 times that of its growth along a linear path.

While crack deflection certainly affects the crack growth rate in this case, the effect cannot be the major source of the reduced crack growth. Crack deflection reduces the growth rate, at most, 1.5 ($=1/0.67$) times, while the experimental data (Figure 3) indicate that the growth rate is reduced by at least a factor of 4 as a result of the transformation. Moreover, the crack propagates through the martensite particles when the transformation in front of it is not extensive. Therefore, the crack deflection effect only applies when ΔK is large.

3. *Work hardening*

The $\gamma \rightarrow \alpha'$ transformation increases the effective rate of work hardening. This effect is apparent in Table II, which includes the ratios of the ultimate and yield strengths. Pineau and Pelloux[4] proposed that an increase in work-hardening rate due to transformation would cause a reduction in the crack growth rate. However, there is no well-developed model that permits us to quantify the effect.

As reviewed by McEvily,[46] the proposed mechanisms of fatigue crack propagation in the Paris region can be divided into two sets. One set focuses on the plastic sliding-off process at the crack tip; the other emphasizes damage accumulation. In the first type of model, the crack growth rate can be related to the crack tip opening displacement (CTOD),

$$\frac{da}{dN} \approx 0.5(\text{CTOD}) = 0.5\left[\frac{\Delta K^2}{E\sigma_y}\right] \quad [25]$$

where σ_y and E are the yield stress and Young's modulus, respectively. In the damage accumulation model, a fatigue crack grows an incremental length, Δa, if a critical value of the accumulated plastic displacement is reached, and

$$\frac{da}{dN} = C\left[\frac{\Delta K^4}{E\sigma_y^3 D_c}\right] \quad [26]$$

where D_c is the critical plastic displacement. Neither of these relations is experimentally verified. However, both imply that an increase in flow stress causes a reduction in the crack growth rate.

The stress and strain fields at a crack tip in a material that exhibits power law hardening ($\sigma = A\varepsilon^n$) under K_I loading have been found[47,48] and are

$$\sigma_{ij} = \left(\frac{1}{r}\right)^{n/(1+n)} \Sigma_{ij}$$
$$\varepsilon_{ij} = \left(\frac{1}{r}\right)^{1/(1+n)} E_{ij} \quad [27]$$

where the matrices Σ_{ij} and E_{ij} are found numerically from the external loading, the work-hardening coefficient, n, the crack orientation, and the elastic constants.[49] Work hardening elevates the stress at the crack tip and raises the ratio of the maximum normal stress to equivalent stress.[47] At the same time, work hardening makes the strain at the crack tip more uniform. For example, in a perfectly plastic material, the strains vary as r^{-1}, while in a hardenable material, the strains vary as $r^{-1/(1+n)}$, where $0 < n < 1$. The plastic zone size decreases as (n) increases.[47]

These analyses suggest that the crack growth rate may vary in either direction with increasing work hardening. Work hardening reduces the CTOD and the plastic zone size, which should decrease the crack growth rate; on the other hand, it enhances the stresses and the normal-to-shear stress ratio, which increases the probability of fracture by cleavage. The net effect is not clear.

4. *Fracture mode transition*

Finally, there is an evident transition in the local mode of fracture when transformation intrudes in the samples studied here. The fatigue fracture surfaces in the samples that did not transform (Figures 10(a) and (b)) are rough and exhibit traces of significant plastic deformation; the surfaces of the samples that did transform (Figures 10(c) through (f)) are flat and show a predominant cleavage or quasi-cleavage fracture mode. It appears that the material becomes brittle after the transformation, which is consistent with the behavior of fresh martensite, and should accelerate crack propagation. The brittleness of the fresh martensite phase may also contribute to the load ratio effect: at low load ratios, the crack growth rate is held down by the compressive residual stress; at high load ratios, the extensive transformation in front of the crack and the high static stress promote a low-energy, brittle fracture. However, the experimental data suggest that this effect is not quantitatively large in these steels; the crack growth rate in the cold-rolled material that contains a high fraction of martensite is similar to that in annealed 304L, as shown in Figure 14(a).

V. CONCLUSIONS

1. The martensitic transformation that occurs at the tip of a growing fatigue crack in metastable 304-type steels significantly reduces the fatigue crack propagation rate in both the threshold and Paris regions. However, the effect decreases as the load ratio, or mean stress, increases.
2. Several mechanisms apparently contribute to the decreased crack growth rate in steels that transform. The most important is the perturbation of the stress field

at the crack tip. By modifying previous theories of the influence of the transformation on the crack tip stress intensity, it is possible to obtain a theory that provides a reasonable quantitative fit to the experimental data. To improve this theory, it is necessary to develop a good quantitative model that includes the net shear due to the martensite transformation. Other factors also contribute to the change in the crack growth rate. These include crack deflection, the increased work-hardening rate, and the relative brittleness of the fresh martensite phase.

ACKNOWLEDGMENTS

The authors are grateful to Professor R.O. Ritchie, Dr. W. Yu, and Dr. J. Shang, Lawrence Berkeley Laboratory, for helpful discussions and assistance in the fatigue tests. This work was supported by the Director, Office of Energy Research, Office of Fusion Energy, Development and Technology Division of the United States Department of Energy, under Contract No. DE-AC03-76SF00098.

REFERENCES

1. J.F. Breedis and W.D. Robertson: *Acta Metall.*, 1962, vol. 10, pp. 1077-88.
2. H. Fiedler, B. Averbach, and M. Cohen: *Trans. ASM*, 1955, vol. 47, pp. 276-90.
3. R. Reed: *Acta Metall.*, 1962, vol. 10, pp. 865-77.
4. A.G. Pineau and R.M. Pelloux: *Metall. Trans.*, 1974, vol. 5, pp. 1103-12.
5. C. Bathias and R.M. Pelloux: *Metall. Trans.*, 1973, vol. 4, pp. 1265-73.
6. R.L. Tobler and R.P. Reed: *J. Test. Eval.*, 1984, vol. 12 (6), pp. 364-70.
7. G. Schuster and C. Altstetter: *Metall. Trans. A*, 1983, vol. 14A, pp. 2077-84.
8. G. Schuster and C. Altstetter: *Fatigue Mechanisms*, ASTM STP 811, ASTM, Philadelphia, PA, 1983, pp. 445-63.
9. G.R. Chanani, Stephen D. Antolovich, and W.W. Gerberich: *Metall. Trans.*, 1972, vol. 3, pp. 2661-72.
10. E. Hornbogen: *Acta Metall.*, 1978, vol. 26, pp. 147-52.
11. A.J. McEvily, W. Zagrany, and J. Gonzalez: in *Basic Mechanisms in Fatigue of Metals*, P. Lukas and J. Polak, eds., Elsevier, New York, NY, 1988, pp. 271-79.
12. G.M. Chang: M.S. Thesis, University of California, Berkeley, CA, 1983.
13. G.H. Eichelman and F.C. Hull: *Trans. ASM*, 1953, vol. 45, pp. 77-104.
14. I. Williams, R.G. Williams, and R.C. Capellaro: *Proc. 6th Int. Cryogenic Engineering Conf.*, IPC Science and Technology Press, Guildford, Surrey, England, 1976, pp. 337-41.
15. *Annual Book of ASTM Standards*, E 647-83, ASTM, Philadelphia, PA, 1983, pp. 739-59.
16. *Metals Handbook*, 9th ed., ASM, Metals Park, OH, 1985, vol. 8, pp. 386-402.
17. M.D. Halliday and C.J. Beevers: in *The Measurement of Crack Length and Shape During Fracture and Fatigue*, C.J. Beevers, ed., Engineering Materials Advisory Services Ltd., West Midlands, United Kingdom, 1981, pp. 85-112.
18. T.C. Lindley: in *Subcritical Crack Growth due to Fatigue, Stress Corrosion and Creep*, L.H. Larsson, ed., Elsevier Applied Science, New York, NY, 1981, pp. 167-213.
19. R.O. Ritchie and W. Yu: in *Small Fatigue Cracks*, R.O. Ritchie and J. Lankford, eds., TMS-AIME, Warrendale, PA, 1986, pp. 167-89.
20. W.F. Deans and C.E. Richards: *J. Test. Eval.*, 1979, vol. 7, pp. 147-54.
21. *Metals Handbook*, 9th ed., ASM, Metals Park, OH, 1985, vol. 9, pp. 63-70.
22. R.J. Gray: *Revealing Ferromagnetic Microstructures with Ferrofluids*, ORNL-TM-368, Oak Ridge National Laboratory, Oak Ridge, TN, Mar. 1972.
23. T.H. Coleman and D.R.F. West: *Met. Technol.*, Feb. 1976, pp. 49-53.
24. B. Yahiaoui and P. Petriquin: *Note Technique RAM (73) 567*, Division de Metallurgie et D'Etude des Combustibles Nucleaires, Centre d'Etudes Nucleaires de Saclay, Saclay, France, Dec. 1973.
25. L.A. James: *Fatigue Crack Growth Measurement and Data Analysis*, ASTM STP 738, ASTM, Philadelphia, PA, 1981, pp. 45-57.
26. J.L. Bernard and G.S. Slama: *Nucl. Technol.*, 1982, vol. 59 (1), pp. 136-47.
27. L.A. James: Report HEDL-TME 75-20, Westinghouse Hanford Company, Richland, WA, Feb. 1975.
28. S. Suresh and R.O. Ritchie: in *Fatigue Crack Growth Threshold: Concepts*, D.L. Davidson and S. Suresh, eds., TMS-AIME, Warrendale, PA, 1984, pp. 227-61.
29. P.L. Mangonon, Jr.: Ph.D. Thesis, University of California, Berkeley, CA, 1968.
30. R.M. McMeeking and A.G. Evans: *J. Am. Ceram. Soc.*, 1982, vol. 65 (5), pp. 242-46.
31. B. Budiansky, J.W. Hutchinson, and J.C. Lambropoulos: *Int. J. Solids Struct.*, 1983, vol. 19 (4), pp. 337-55.
32. J.C. Lambropoulos: *Int. J. Solids Struct.*, 1986, vol. 22 (10), pp. 1083-1115.
33. N.I. Muskhelishvili: *Some Basic Problems of the Mathematical Theory of Elasticity*, P. Noordhoff Ltd., Groningen, The Netherlands, 1953, pp. 225-27.
34. H. Tada, P.C. Paris, and G.R. Irwin: *The Stress Analysis of Cracks Handbook*, Del Research Corporation, Hellertown, PA, 1973, pp. F.1-F16 and C.1-C20.
35. J.D. Eshelby: *Proc. R. Soc. London*, 1957, vol. A241, pp. 376-96.
36. P.C. Paris, R.M. McMeeking, and H. Tada: *Cracks and Fractures*, ASTM STP 601, ASTM, Philadelphia, PA, 1976, pp. 471-89.
37. S. Chen, A.G. Khachaturyan, and J.W. Morris, Jr.: *Proc. ICOMAT 1979*, W.S. Owen, ed., Massachusetts Institute of Technology, Cambridge, MA, 1980, pp. 94-99.
38. K. Katagiri, M. Tsuji, T. Okada, K. Ohji, R. Ogawa, G.M. Chang, and J.W. Morris, Jr.: *Adv. Cryog. Eng.*, 1989, vol. 36, pp. 1225-32.
39. R.O. Ritchie: Class Notes of MSE 212, available in the Engineering Library, University of California, Berkeley, CA, 1987.
40. Dr. K. Chang: General Electric Company, Fairfield, CT, and Dr. R. Sawtell, Aluminum Company of America, Alcoa Center, private communication, 1989.
41. S. Suresh: *Metall. Trans. A*, 1983, vol. 14A, pp. 2375-85.
42. A.A. Khrapkov: *Int. J. Fract. Mech.*, 1971, vol. 7, pp. 373-82.
43. B.A. Bilby, G.E. Cardew, and I.C. Howard: in *Fracture 1977*, D.M.R. Taplin, ed., University of Waterloo Press, PO, Canada, 1977, vol. 3, pp. 197-200.
44. B. Cotterell and J.R. Rice: *Int. J. Fract.*, 1980, vol. 16, pp. 155-69.
45. P.C. Paris and G.C. Sih: *Stress Analysis of Cracks*, ASTM STP 381, ASTM, Philadelphia, PA, 1965, pp. 30-40.
46. A.J. McEvily: *Fatigue Mechanisms*, ASTM STP 811, ASTM, Philadelphia, PA, 1983, pp. 283-312.
47. J.R. Rice and G.F. Rosengren: *J. Mech. Phys. Solids*, 1968, vol. 16, pp. 1-12.
48. J.W. Hutchinson: *J. Mech. Phys. Solids*, 1968, vol. 16, pp. 13-31.
49. A.G. Evans and R.M. Cannon: *Acta Metall.*, 1986, vol. 34, pp. 761-800.
50. B.D. Marshall, A.G. Evans, and M. Drory: in *Fracture Mechanics of Ceramics*, R.C. Bradt, A.G. Evans, D.P.H. Hasselman, and F.F. Lange, eds., Plenum Press, New York, NY, 1983, vol. 6, pp. 289-307.
51. M. Ruhle: University of California at Santa Barbara, Santa Barbara, CA, unpublished research, 1983.
52. A.G. Evans, Z.B. Ahmad, D.G. Gilbert, and P.W.R. Beaumont: *Acta Metall.*, 1986, vol. 34, pp. 79-87.